analytical chemistry

pubs.acs.org/ac

Article

Supramolecular Mimotope Peptide Nanofibers Promote Antibody−Ligand Polyvalent and Instantaneous Recognition for Biopharmaceutical Analysis

Qiaoxian He, Feng Chen, Zheng Zhao, Pengfei Pei, Yongqing Gan, Aixuan Zhou, Jingwei Zhou, Jia-Huan Qu, Jacques Crommen, Marianne Fillet, Yingchun Li,* Qiqin Wang,* and Zhengjin Jiang*

Cite This: https://doi.org/10.1021/acs.analchem.4c00051

Read Online

ACCESS | Metrics & More | Article Recommendations | Supporting Information

ABSTRACT: Peptide-based supramolecules exhibit great potential in various fields due to their improved target recognition ability and versatile functions. However, they still suffer from numerous challenges for the biopharmaceutical analysis, including poor self-assembly ability, undesirable ligand−antibody binding rates, and formidable target binding barriers caused by ligand crowding. To tackle these issues, a "polyvalent recognition" strategy employing the CD20 mimotope peptide derivative NBD-FFVLR-GS-WPRWLEN (acting on the CDR domains of rituximab) was proposed to develop supramolecular nanofibers for target antibody recognition. These nanofibers exhibited rapid self-assembly within only 1 min and robust stability. Their binding affinity (179 nM) for rituximab surpassed that of the monomeric peptide (7 μM) by over 38-fold, highlighting that high ligand density and potential polyvalent recognition can efficiently overcome the target binding barriers of traditional supramolecules. Moreover, these nanofibers exhibited an amazing "instantaneous capture" rate (within 15 s), a high recovery (93 ± 3%), and good specificity for the target antibody. High-efficiency enrichment of rituximab was achieved from cell culture medium with good recovery and reproducibility. Intriguingly, these peptide nanofibers combined with bottom-up proteomics were successful in tracking the deamidation of asparagine 55 (from 10 to 16%) on the rituximab heavy chain after 21 day incubation in human serum. In summary, this study may open up an avenue for the development of versatile mimotope peptide supramolecules for biorecognition and bioanalysis of biopharmaceuticals.

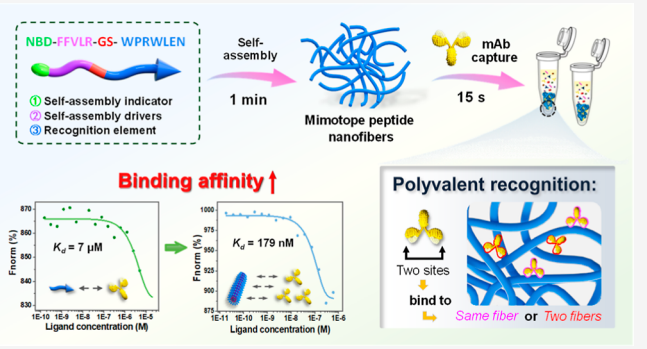

INTRODUCTION

Peptides are fundamental components of cells and tissues and play key roles in nearly all biological activities. Inspired by the nature's evolution of function through superstructure formation, a range of peptide-based supramolecules (such as nanofibers, nanotubes, and nanovesicles) have been developed by self-assembly of peptides with multiple functional modules.[1] Depending on their superior target recognition ability, in vivo circulation, cell permeability, and tissue penetration, peptide-based supramolecules exhibited tremendous potentials in biotherapy, tissue engineering, bioimaging, and bioseparation.[2] For biotherapy, the self-assembled peptide−drug conjugate SAP-CPT with a cytotoxic payload (CPT) and an integrin $\alpha v\beta 3$ receptor can specifically target tumor cells and self-assemble in situ into nanofibers, thereby significantly improving the cell permeability and bioavailability and thus expanding the therapeutic window.[3] Moreover, the multi-epitope (EGFRvIII epitope of the B cell, Trp2 epitope of the $CD8^+$ T cell, and Td epitope of the $CD4^+$ T cell) supramolecular peptide nanofibers can be developed as epitope-specific vaccines to elicit coordinated humoral and cellular antitumor immune responses for the improvement of antitumor functions of vaccine-induced antibodies.[4] More importantly, with the rapid development of biopharmaceuticals, the peptide Z33-based supramolecule, which can recognize the fragment crystallizable region (Fc) of the antibody, was explored as an affinity precipitant to purify the therapeutic monoclonal antibody (mAb) from CHO cell cultural media with a good recovery (88%).[5,6] Therefore, peptide-based supramolecules could in the future lead to decisive advances in various fields, thanks to the directed functional evolution made possible by self-assembly.

However, some peptide-based supramolecules may suffer from a series of inherent obstacles, including low self-

Received: January 3, 2024
Revised: March 3, 2024
Accepted: March 22, 2024

Scheme 1. Design of Supramolecular Mimotope Peptide Nanofibers (MPFs) for Antibody Recognition and Capture

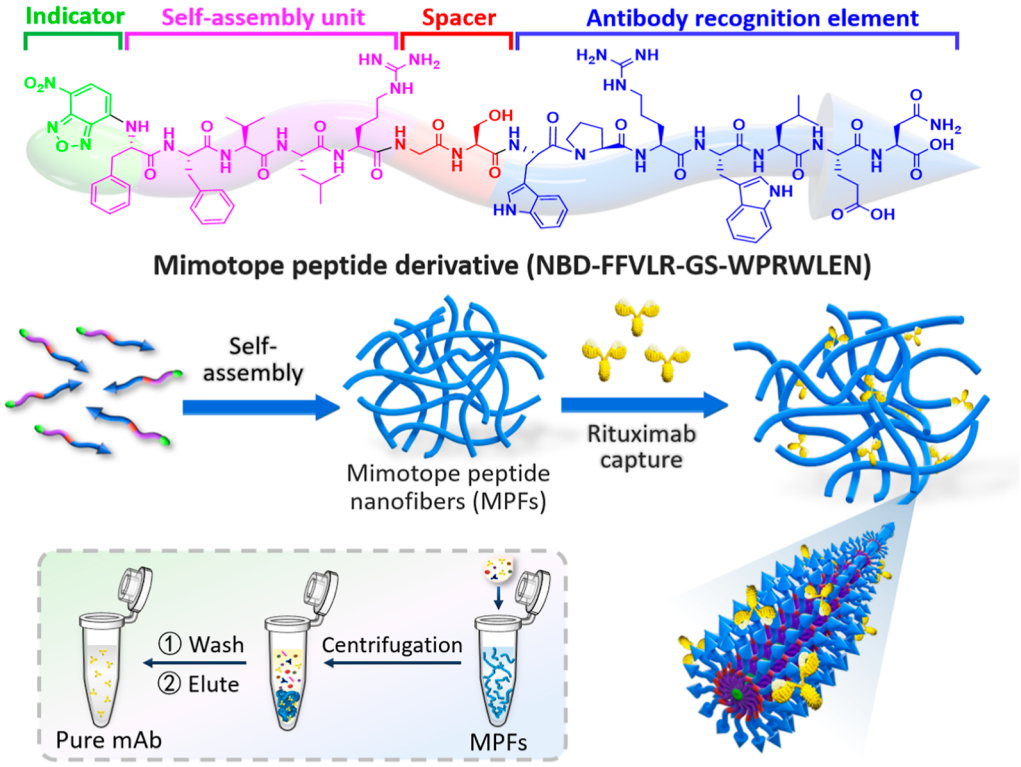

assembling efficiency (antiCD3-G7-RGD's assembly $t_{1/2}$ = 86 min, SAP-CPT's assembly $t_{1/2}$ = 2575 min)[2,3] and reversible assembly, which may reduce the supramolecule's stability.[7,8] Furthermore, the superstructures of preassembled biomaterials could be altered in complex physiological environments, compromising properties and/or biofunctions.[9] Most of all, for antibody recognition, the C12-Z33 supramolecular nanofiber exhibited a 10-fold lower affinity than the monomeric peptide Z33,[5] indicating that outstanding binding site barriers between the C12-Z33 supramolecule and the antibody are due to peptide ligand overcrowding. To fine-tune their binding behavior, more complex supramolecular copolymers, formed by the coassembly of the filler (C12-VVEE) and ligand (C12-VVKKGGZ33) at different molar ratios, were developed to modulate the density of Z33 on the supramolecular surface and optimize the performance of the protein−supramolecule precipitate for mAb purification.[6] Although exhibiting good binding performance, the protein−supramolecule precipitates formed had to be obtained by high-speed centrifugation (15,000 rpm, 10 min), redissolved, and then subjected to a time-consuming membrane separation process (48 h) to remove the filler and peptide ligands for mAb recovery. So, improving their self-assembling ability, stability, and ligand−target protein binding mechanism remains a major challenge for practical supramolecular applications.

Peptide self-assembly is a spontaneous thermodynamic and kinetic driven process based on the synergistic effect of numerous noncovalent intermolecular interactions, such as hydrogen bonding, hydrophobic interaction, electrostatic interaction, van der Waals, and $\pi-\pi$ stacking.[10,11] Therefore, rational peptide sequence design is of great importance for the formation of the desired morphology to achieve controllable self-assembly.[12] The strong hydrogen bonding and hydrophobic interactions between peptides were found to drive rapid self-assembly and maintain excellent stability within biological systems.[13−15] For example, the highly hydrophobic FFVLK instead of hydrophilic GGAAK nearly doubled the self-assembly capacity [critical assembly concentration (CAC) decreased from 7.0 μM to 4.2 μM].[16] The self-assembly performance parameters of amyloid peptides with strong hydrogen bonds are 1 to 2 orders of magnitude higher than those of peptides without hydrogen bonds.[13,17] More interestingly, to improve the binding capacity of supramolecules to target the mAb and even their specificity for bioanalysis, a "polyvalent recognition" strategy based on the antigen mimotope peptide was proposed in this study. Mimotope peptides, as promising "surrogate antigens", can bind specifically to the complementarity determining regions (CDRs) of the corresponding mAb.[18−22] Therefore, perhaps the two CDR binding sites of the target mAb were coanchored on the same supramolecule or on two adjacent supramolecules, which could activate "polyvalent recognition" for the antibody to overcome traditional supramolecule binding site barriers and even enhance binding affinity.[23,24] However, no supramolecules based on mimotope peptides have been reported to date.

In this study, to drive applications of supramolecules in the biopharmaceutical field, based on the "polyvalent recognition" strategy and unique advantages of the mimotope peptide, the CD20 mimotope peptide derivative (NBD-FFVLR-GS-WPRWLEN) functionalized supramolecular nanofibers were first designed for rituximab recognition (rituximab is approved for the treatment of non-Hodgkin's lymphomas, Scheme 1). Introducing the hydrophobic nitrobenzoxadiazole (NBD) and the GS linker could further strengthen interactions between FFVLR molecules (similar to those of KLVFF), triggering the highly efficient self-assembly of mimotope peptide derivatives and ensuring their stability in complex biofluids. The abundant

https://doi.org/10.1021/acs.analchem.4c00051
Anal. Chem. XXXX, XXX, XXX−XXX

mimotope peptide WPRWLEN as recognition elements on the surface of supramolecules will not only promote "polyvalent recognition" toward the two CDR sites of rituximab but also improve binding rates between the supramolecule and antibodies to achieve "instantaneous capture". Based on this design, the morphology, self-assembly ability, stability, and binding affinity of mimotope peptide derivative-functionalized supramolecules were systematically characterized and evaluated by transmission electron microscopy (TEM), CAC determination, coarse-grained (CG) simulation, dynamic light scattering (DLS), and microscale thermophoresis (MST). Moreover, under the optimal conditions, a new enrichment method was constructed based on this supramolecule to enrich rituximab from cell cultural medium. This enrichment method was also explored for the first time to combine trypsin digestion and liquid chromatography quadrupole time-of-flight mass spectrometry (LC-QTOF-MS) for follow-up analysis of the asparagine 55 modification at the rituximab heavy chain level. Finally, the prospects for developing mimotope peptide-functionalized supramolecules were also considered.

EXPERIMENTAL SECTION

Characterization of Peptide Self-Assembly. Fluorescence assays were run on a microplate reader to characterize the peptide self-assembly. Due to poor water solubility, the mimotope peptide derivatives were first completely dissolved in dimethyl sulfoxide (DMSO) (as the optimal cocosolvent shown in Figure S1) and then diluted to the desired concentration with water. The final solution maintained a fixed 5% DMSO content. The excitation spectrum showed a maximum excitation at 470 nm (Figure S2). Emission spectra were collected in the range from 500 to 700 nm. To determine the CACs, the peptides were diluted until the fluorescence disappeared. CACs were found according to the intersection point of the piecewise linear fit of fluorescence and peptide concentration (see Text S2). The self-assembly speed of the mimotope peptide derivatives into nanofibers was determined by fluorescence time kinetics and CG simulation (details in Text S2).

Affinity Analysis by MST. MST analysis was used to compare the affinity of MPFs and recognition element WPRWLEN to rituximab. For the MPFs, MST experiments can be performed directly due to the fluorescence of NBD. Sixteen rituximab test solutions (from 0.12 μM to 18.3 nM) were obtained by multiple 1:1 dilution of 0.12 μM stock solution using deionized water. 10 μL of 100 nM MPFs was mixed with 10 μL of the 16 rituximab solutions at different concentrations. After incubation at room temperature for 10 min, the solution was transferred to a capillary for MST detection in the nanoblue mode. The dissociation constants (K_d) were obtained by processing the data using the MO. Affinity Analysis Software. For the WPRWLEN recognition element, the analysis must be performed with the aid of fluorescent dye-labeled rituximab. Therefore, rituximab was labeled using a Cy5 antibody labeling kit and finally diluted to 328 nM with water. The WPRWLEN recognition elements were prepared as a 10 μM stock solution in water. Then, serial dilutions of the peptide stock solution, incubation with the labeled rituximab, and MST analysis were performed as described above, though measured in the nanored mode.

Specificity Assessment of the Mimotope Peptide Nanofibers. Fluorescein isothiocyanate (FITC)−human serum albumin (HSA) and Cy5-rituximab were used to evaluate the specific binding ability of the mimotope peptide nanofibers to rituximab. 1.5 mg/mL mimotope peptide nanofibers (100 μL) were incubated with 2 mg/mL FITC−HSA (50 μL) and 0.47 mg/mL Cy5-rituximab (50 μL). The two peptide−protein mixtures were each mixed in a vortex mixer for 15 s, and then, the supernatant and precipitate were separated by centrifugation (3500 rpm, 2 min). The same concentration of two fluorescent protein samples was prepared in water as the control. The above control, supernatant, and precipitate were observed with an in vivo imaging system to acquire fluorescence images. In parallel, the interference of HSA during enrichment was further tested by the enrichment experiment in the HSA−rituximab mixture (methods are depicted in Text S2).

Enrichment of Rituximab Using the Nanofibers in Complex Biofluids. Rituximab (10 μL, 10 mg/mL) was added into the lymphocarcinoma 1640 cell culture medium or 10% serum of healthy people (190 μL) to yield 0.5 mg/mL rituximab-spiked samples. The mimotope peptide nanofibers were prepared as a stock solution of 1.5 mg/mL and allowed to stand for 1 min, and then, they were used immediately. Then, 200 μL of mimotope peptide nanofibers was mixed and vortexed with 100 μL of the spiked sample for 15 s at room temperature, followed by centrifugation (3500 rpm, 2 min) for separation. After removing the supernatant, the precipitate was washed with the wash buffer and separated by centrifugation again. After three repetitions, rituximab was eluted (twice) and collected. The recovery, structure, and purity were investigated by a BCA protein concentration assay kit, circular dichroism (CD), size exclusion chromatography (SEC), and a SCIEX ZenoTOF 7600 mass spectrometer (details in Text S2).

Biotransformation Evaluation of Rituximab by Peptide Mapping Analysis. To simulate and evaluate the biotransformation of rituximab in vivo, the rituximab was first incubated in 10% human serum at 37 °C (final concentration = 0.5 mg/mL). After 21 days, they were enriched using the mimotope peptide nanofibers and digested by trypsin into peptides (rituximab/trypsin = 25:1, 3 h, the digestion was terminated by 0.5% formic acid) for peptide mapping analysis to study their modification of asparagine 55 at the heavy chain. The peptide mapping was analyzed employing an AB Sciex ExionLC system connected to a SCIEX X500R QTOF mass spectrometer using an Acquity BEH C18 column (Waters, ACQUITY UPLCBEH C18 1.7 μm, 2.1 × 150 mm). Specific experimental procedures and conditions, including antibody denaturation, digestion, and LC system and MS parameters, were described in a previous work.[20]

All the experiments were carried out in triplicate, each time producing a new batch of mimotope peptide nanofibers.

RESULTS AND DISCUSSION

Design of Supramolecules and Characterization of Peptide Self-Assembly. To realize the polyvalent and instantaneous recognition of the antibody and cope with the challenges of supramolecules in biopharmaceutical applications, a hydrophobic mimotope peptide derivative with four functional domains (NBD-FFVLR-GS-WPRWLEN) was designed for the first time. As an analogue of FFVLK, the abundant hydrogen bonds, $\pi-\pi$ stacking, and hydrophobic interactions between FFVLR molecules can trigger rapid assembly between mimotope peptide derivatives to form supramolecular nanostructures.[25,26] Moreover, the high-affinity mimotope peptide WPRWLEN served as a recognition

https://doi.org/10.1021/acs.analchem.4c00051
Anal. Chem. XXXX, XXX, XXX−XXX

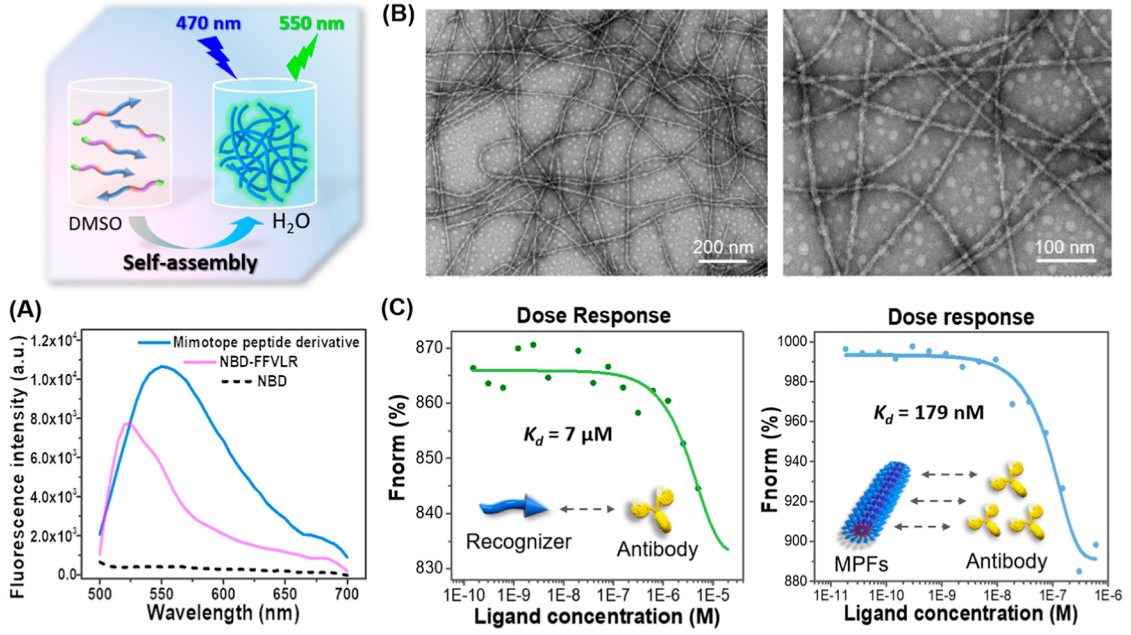

Figure 1. Self-assembly characterization of the mimotope peptide derivatives. (A) Fluorescence spectra of the mimotope peptide derivative (at 254 μM), NBD-FFVLR (at 296 μM), and NBD (at 501 μM). (B) Morphology verification of mimotope peptide nanofibers with TEM. (C) Affinities studies of the recognition element WPRWLEN and MPFs for rituximab by MST.

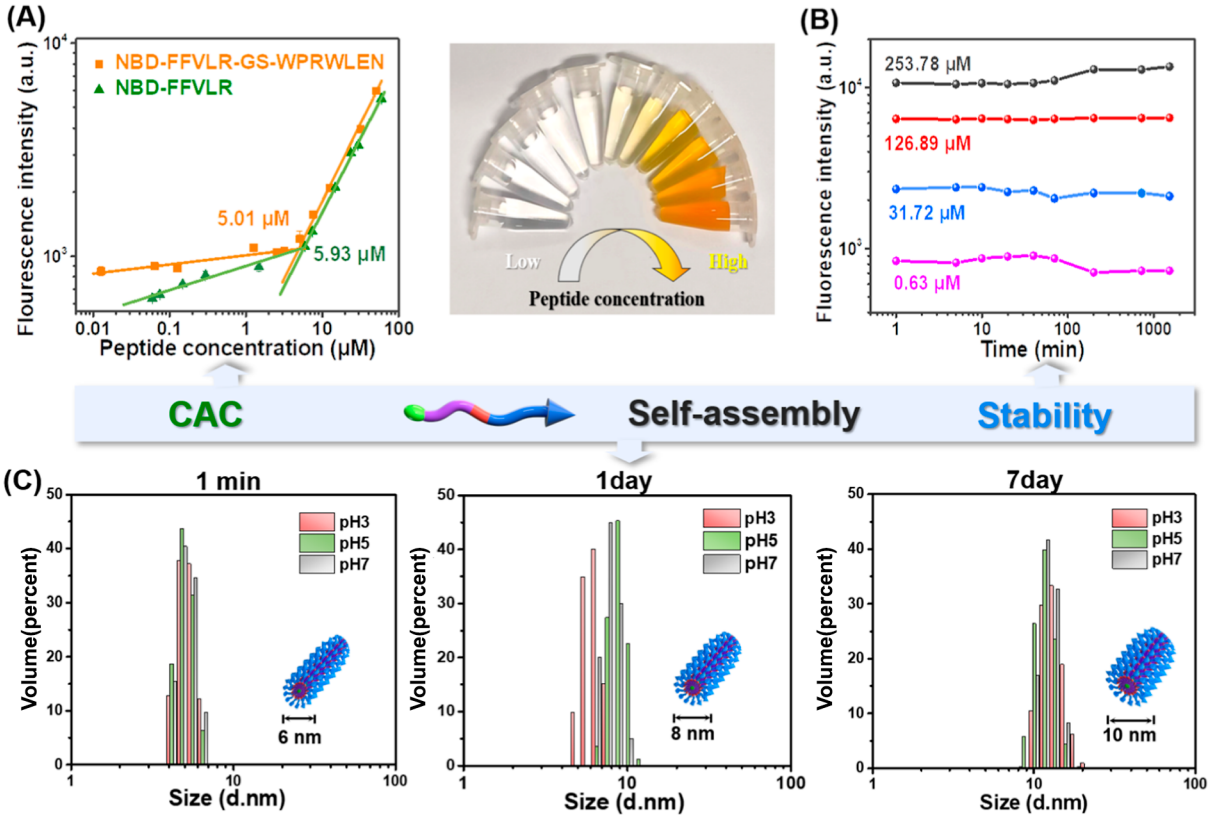

Figure 2. Evaluation of self-assembly ability and stability of the mimotope peptide nanofibers. (A) CAC determination for two peptides (NBD-FFVLR and mimotope peptide derivates). The right image shows the color change of peptide solutions from low to high concentrations. (B) Time kinetics of self-assembly for mimotope peptide derivatives at various concentrations. (C) DLS analysis depicting the sizes (diameters) of mimotope peptide nanofibers at different times and pH levels.

element of target rituximab and was coupled to FFVLR by the GS linker. Furthermore, an additional hydrophobic NBD molecule was used to monitor the self-assembly process as its fluorescence is significantly enhanced with the formation of hydrophobic assembly cores.[3] For comparison, the high-hydrophobic self-assembly unit (NBD-FFVLR) was also synthesized as a positive control. Interestingly, although NBD does not fluoresce, very strong fluorescence was observed

https://doi.org/10.1021/acs.analchem.4c00051
Anal. Chem. XXXX, XXX, XXX−XXX

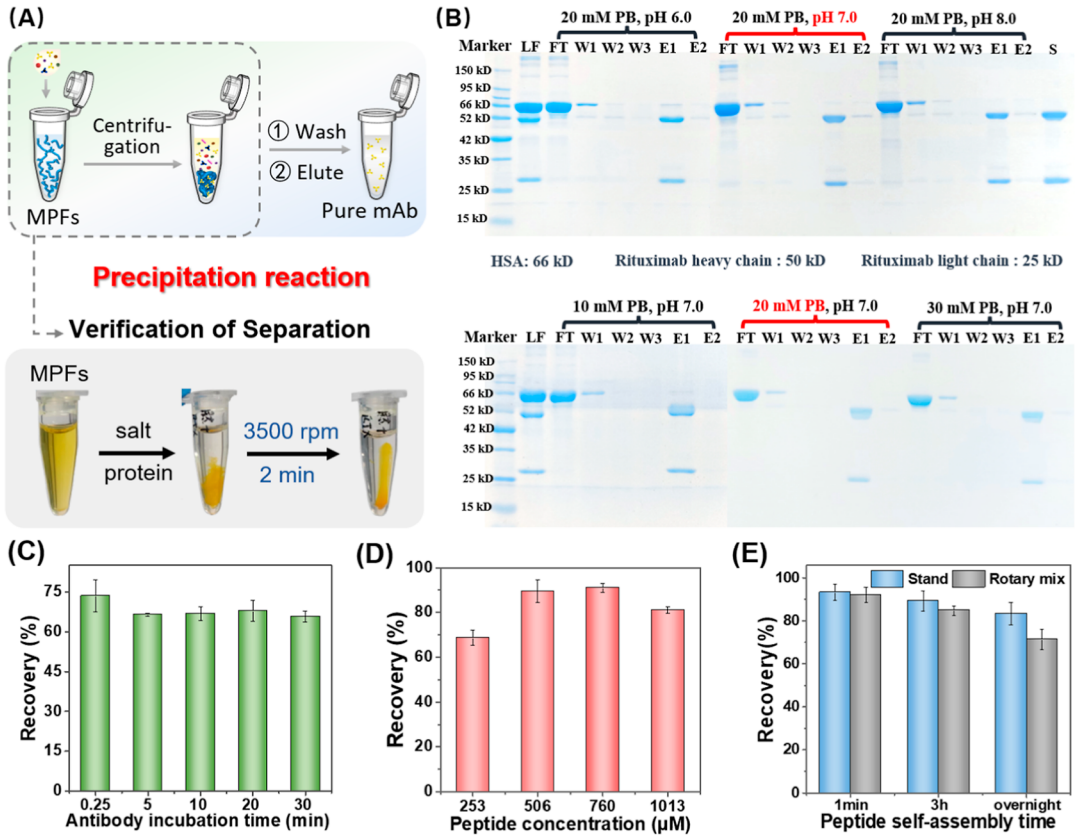

Figure 3. Implementation and optimization of antibody enrichment methods based on the mimotope peptide nanofibers. (A) Feasibility of precipitation-based separation and antibody enrichment processes using the mimotope peptide nanofibers. (B) Optimizations of conditions, including salt concentration and pH of washing buffer. SDS-PAGE channel: LF, loading fraction; FT, flow-through from mimotope peptide nanofibers; W1−3, washing fractions 1−3; E1−2, elution fractions 1−2; and S, standard rituximab. Optimization of the antibody incubation time (C), MPFs concentration (D), and self-assembly time and mixing mode of the MPFs (E).

in self-assembled NBD-FFVLR nanofibers (Figure 1A). Fluorescence activation may be due to the fact that peptide self-assembly creates a hydrophobic environment for NBD, resulting in remarkable fluorescence effects, similar to aggregation-induced emission features.[27] Based on the strong fluorescence emission at 550 nm of the mimotope peptide derivative, a more significant self-assembly event was observed when its DMSO solution was diluted with water. TEM results demonstrated the existence of supramolecular nanofibers (Figure 1B). The mimotope peptide derivatives showed a clear nanofiber structure with an average diameter of around 10 nm, and a large number of fibers were wound around each other to form a network. Given that abundant high-affinity recognition elements (WPRWLENs) could be exposed in an ordered fashion on the surface of the mimotope peptide nanofibers, we hypothesized that two CDR binding sites of the target antibody could be coanchored on the same fiber or on two adjacent fibers, thus promoting "polyvalent recognition" of the antibody and increasing the binding affinity. To confirm the hypothesis, the binding affinities of WPRWLEN−rituximab and supramolecular nanofibers−rituximab were measured by MST and compared. From these fitting curves shown in Figure 1C, the affinities (K_d values) of the recognition element WPRWLEN and the mimotope peptide nanofibers for rituximab were 7 μM and 179 nM, respectively. The affinity of the nanofibers was about 38-fold (calculated at K_d) higher than that of the monomeric recognition element, demonstrating the potential polyvalent recognition between the nanofibers and rituximab. This polyvalent recognition effect transforms the high ligand density of peptide supramolecules from a disadvantage to an advantage, facilitating antibody binding and addressing the binding barrier issue in traditional supramolecules. These characteristics render them promising for antibody capture from biosamples. However, inefficient self-assembly and low stability of supramolecular peptide nanofibers could limit their practical applications in complex biosystems.[28]

Thus, the CAC of the mimotope peptide derivative was then determined based on the fluorescence responsiveness of NBD to assess the self-assembly capacity. As shown in Figure 2A, the measured CACs for mimotope peptide derivatives and NBD-FFVLR were 5 μM and 6 μM, respectively, which were significantly lower than those of many reported self-assembly molecules (such as C16-V_4K_4GKKKRAAK, CAC = 45 μM; AKMGEGGWGANDY-GNNQQNY-RGD, CAC = 33 μM; and FFYEEEG, CAC = 29 μM, Table S1), indicating that the mimotope peptide derivative possesses superior self-assembly ability. This strong assembly ability could be attributed to the abundant intermolecular interactions of NBD-FFVLR-GS-WPRWLEN, such as hydrogen bonds for orientation-induced assembly, $\pi-\pi$ interactions, and hydrophobic interactions of aromatic residues stabilizing the assembly.[10] In addition, due to the clear segmentation of hydrophilic and hydrophobic regions, the mimotope peptide derivatives tend to assemble in the form of hydrophilic tails WPRWLENs outside and hydrophobic units inside to maintain their stability in an

https://doi.org/10.1021/acs.analchem.4c00051
Anal. Chem. XXXX, XXX, XXX−XXX

aqueous environment. These factors enable mimotope peptide derivatives to self-assemble despite a low concentration.

High assembly capability is also expected to be accompanied by rapid assembly and a stable superstructure.[29] Consequently, the assembly speed and stability of nanofibers were evaluated by the subsequent self-assembly kinetics analysis. As shown in Figure 2B, no obvious increase or decrease in the fluorescence of mimotope peptide nanofibers was observed at different concentrations within 25 h. The phenomenon demonstrated that the mimotope peptide derivatives could self-assemble within only 1 min and exist very stably in aqueous solution for a long time. The size of the mimotope peptide nanofibers grew from 6 nm to about 10 nm within 7 days at different pHs, indicating that they did not depolymerize (Figure 2C).

Given the speed of assembly, the self-assembly process of the mimotope peptide derivatives was explored and visualized by a CG simulation based on the MARTINI force field. Equilibrium mimotope peptide derivatives were first simulated by solvation, and various numbers of coarse grain peptides were placed in 60 × 20 × 20 nm boxes corresponding to concentrations of 25, 50, or 100 μM. In the 4×10^6 ps simulation experiment, the peptide clusters decreased rapidly during the first 1×10^6 ps and then slowly until the end (Figure S3). This phenomenon revealed that the self-assembly process of the mimotope peptide derivatives is divided into two steps. The high concentration of mimotope peptide derivatives could assemble into nanofibers within only 2 μs, while the low concentration of mimotope peptide derivatives assembled into nanoclusters within 4 μs, indicating that the higher the concentration of mimotope peptide derivatives, the faster the assembly rate. These results confirmed the "rapid self-assembly" of mimotope peptide derivatives at high concentrations. Moreover, the internal interactions analysis of these assembly structures indicated that the abundant hydrogen bonds and $\pi-\pi$ interactions between peptide derivatives will contribute toward their rapid self-assembly to form nanofibers (Figure S4). Thanks to their high self-assembly capacity and good stability, the preparation of mimotope peptide nanofibers is very simple and convenient, which can facilitate the implementation of a high-efficiency enrichment method for biopharmaceutical analysis.

Implementation and Optimization of Antibody Enrichment Methods. To explore the feasibility of developing a substrate-free enrichment method based on the mimotope peptide nanofibers in biological systems, the precipitation reaction of nanofibers with proteins in salt solution was first verified (Figure 3A). The nanofibers precipitated clearly after adding the salt-containing proteins, and the protein−nanofiber mixtures were easily separated from the solution by low-speed and short-time centrifugation (3500 rpm, 2 min, a condition set to avoid the self-precipitation of macromolecular protein). Based on this, a simple substrate-free antibody enrichment method was developed. Various parameters affecting the enrichment efficiency of mimotope peptide nanofibers were then optimized in-depth. The washing step is essential to remove impurities from complex samples.[30] According to previous studies, an appropriate salt concentration (20 mM PB) and pH (8.0) can increase the surface tension of the solution and reduce electrostatic interactions with interfering proteins.[31] Therefore, the salt concentration (from 10 to 30 mM PB) and pH (from 6.0 to 8.0) of the washing buffer were systematically studied to ensure selective retention of antibodies. As shown in Figure 3B, HSA could not be completely removed at low concentrations of salt and pH, while too high concentrations of salt and pH resulted in the leakage of rituximab. At 20 mM PB and pH 7.0, the mimotope peptide nanofibers exhibited the highest recovery (85%) for rituximab and a satisfactory antifouling ability for HSA, so it was selected as the optimal washing condition for subsequent studies.

To investigate the influence of nanofibers−antibody incubation time[32,33] on the enrichment performances, the recovery of rituximab was measured at several times (15 s, 5 min, 10 min, 20 min, and 30 min) under agitation (Figure 3C). Interestingly, the capture of rituximab was achieved within only 15 s, whereas additional incubation did not result in a higher recovery. This indicated that mimotope peptide nanofibers can capture antibodies at an amazing speed and can be described as "instantaneous capture", which is much faster than most enrichment methods reported to date[22] (data comparison in Table S2). We hypothesized that "instantaneous capture" could be attributed to the enhancement of some properties arising from peptide self-assembly, such as high affinity (K_d = 179 nM) and ligand densities, and even polyvalent recognition.

Another key parameter was investigated, namely, the mimotope peptide nanofibers concentration (from 253 to 1013 μM). As expected, increasing the concentration of mimotope peptide nanofibers was accompanied by improved recovery (Figure 3D). However, when the concentration reached 1013 μM, recovery began to decrease, indicating that a high concentration was not conducive to antibody enrichment, which might be due to space crowding caused by excessive self-assembly and winding of peptide fibers in this case. Therefore, 760 μM with the highest recovery (91 ± 2%) was chosen as the final concentration of the mimotope peptide nanofibers.

Finally, the self-assembly time and mixing mode (standing and rotary mixing) of the mimotope peptide derivatives were also explored (Figure 3E). Noticeably, the enrichment efficiency was the highest (93 ± 4%) at 1 min of self-assembly for the mimotope peptide nanofibers but decreased with the increasing assembly time. This downward trend was more pronounced with the rotary mixing mode, probably because the mimotope peptide nanofibers assemble too quickly in this mode and coil into clusters (it was identified and shown in Figure S5), resulting in part of the binding sites being embedded, so that antibodies cannot efficiently bind in a short time. Eventually, standing for 1 min was selected as the optimal preparation method of mimotope peptide nanofibers. Under optimal conditions, the mimotope peptide nanofibers exhibit instantaneous capture and high enrichment yields, overcoming the drawbacks of low capture efficiency observed with previously reported affinity materials[34−36] and showing potential to be advantageous in practical applications. Moreover, the remaining nanofibers after enrichment could be recycled back into an aqueous solution and reused for additional enrichment cycles (up to three times).

Specificity Assessment of the Mimotope Peptide Nanofibers for Antibody Enrichment. Excellent specificity is an essential prerequisite for good recognition and capture of target proteins in complex biosamples. First, to visually compare the adsorption behavior of mimotope peptide nanofibers to rituximab and nonspecific interference HSA, two fluorescent proteins (FITC−HSA and Cy5-rituximab) were coprecipitated with the mimotope peptide nanofibers. After washing, the fluorescence changes in the supernatant and nanofiber precipitate were observed. As shown in Figure 4A,

https://doi.org/10.1021/acs.analchem.4c00051
Anal. Chem. XXXX, XXX, XXX−XXX

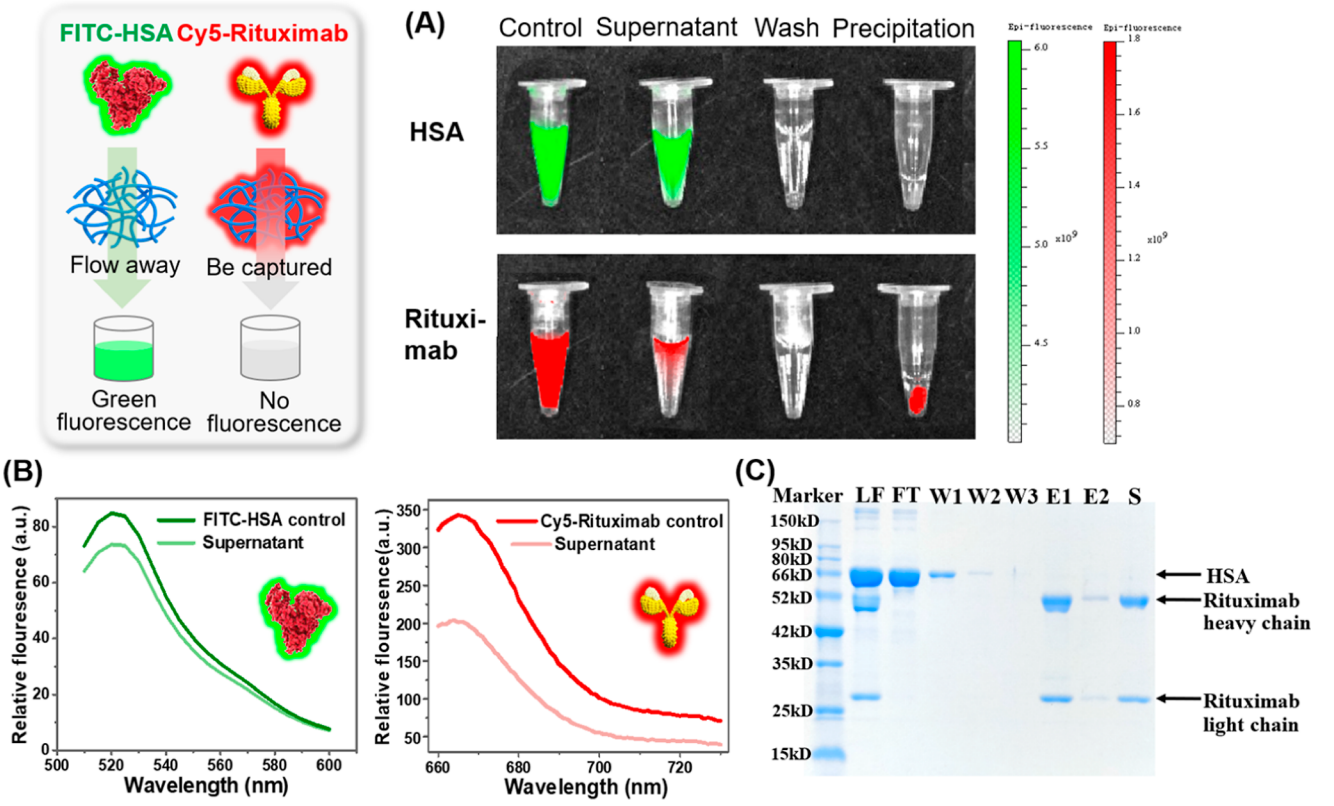

Figure 4. Specificity assay of the mimotope peptide nanofibers for rituximab. (A) Fluorescence images and (B) determination of different components obtained by precipitation of FITC−HSA and Cy5-rituximab with mimotope peptide nanofibers. (C) SDS-PAGE analysis for the enrichment of the protein mixture (HSA/rituximab = 2 mg/mL/0.5 mg/mL) under optimal conditions. Channel: LF, loading fraction; FT, flow-through from mimotope peptide nanofibers; W1−3, washing fractions 1−3; E1−2, elution fractions 1−2; and S, standard rituximab.

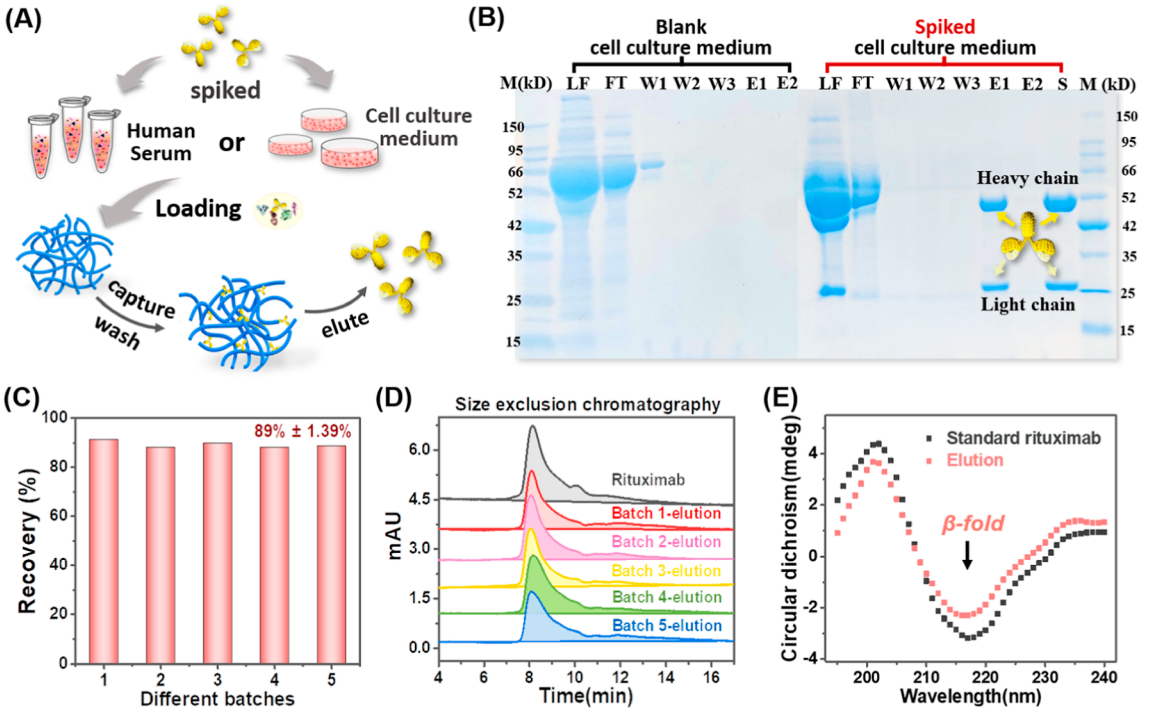

Figure 5. Applications of the mimotope peptide nanofibers in complex samples. (A) Antibody purification procedures from two biofluids. (B) Enrichment of rituximab by the mimotope peptide nanofibers in cancer cell culture medium. SDS-PAGE channel: LF, loading fraction; FT, flow-through from mimotope peptide nanofibers; W1−3, washing fractions 1−3; E1−2, elution fractions 1−2; and S, standard rituximab. (C) Repeatability evaluation of enrichment using multiple-batch mimotope peptide nanofibers. (D) SEC of standard rituximab and the 5 elution fractions. (E) CD of the eluent and 0.2 mg/mL standard rituximab in the same buffer: pH 3.0, 10 mM HCOONa, 100 mM NaCl.

https://doi.org/10.1021/acs.analchem.4c00051
Anal. Chem. XXXX, XXX, XXX−XXX

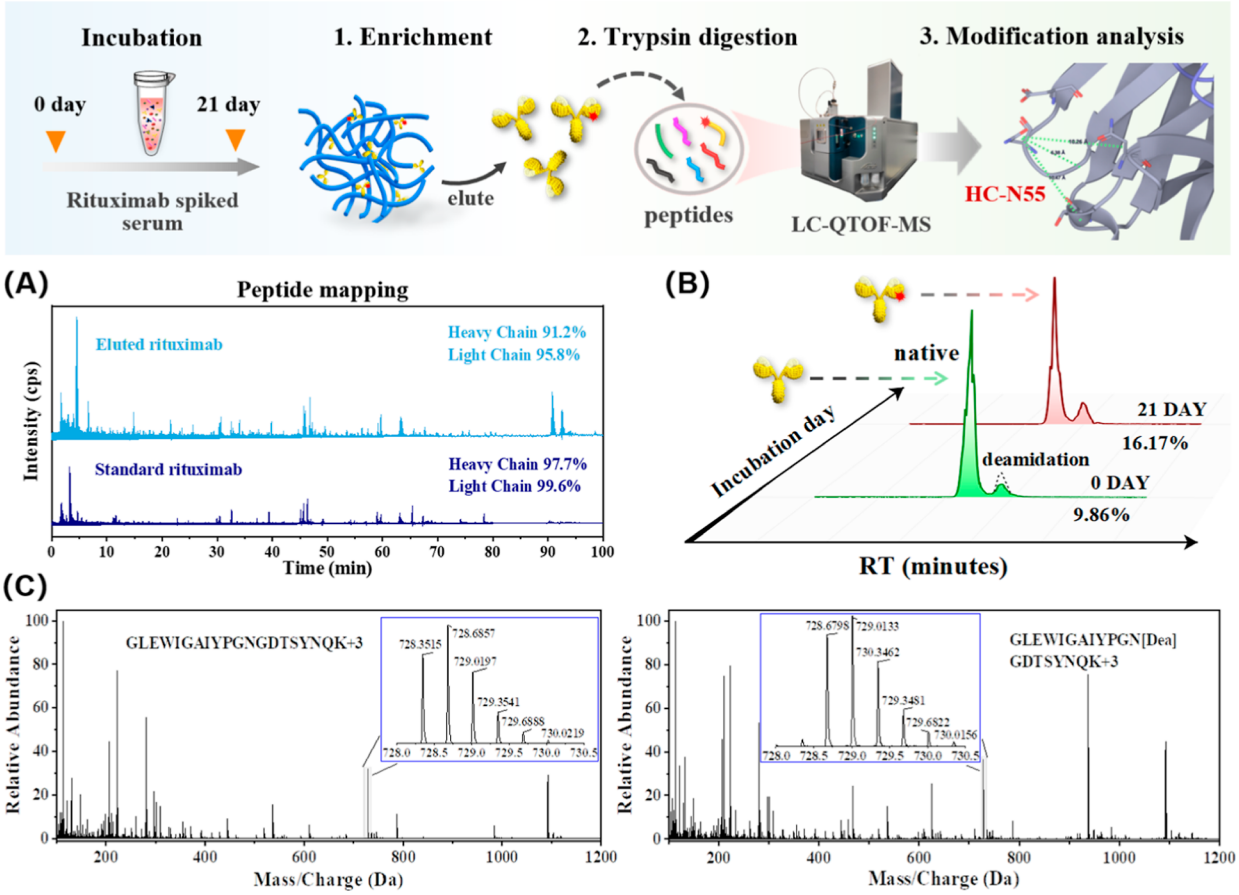

Figure 6. PTM analysis of rituximab in 10% human serum. (A) Peptide mapping of the standard rituximab and eluted rituximab. (B) SEC chromatograms of target peptides at day 0 and day 21. (C) Mass spectrometry of deamidation modification on the heavy chain of rituximab after 21 day incubation in human serum.

the FITC−HSA was only present in the supernatant, with no obvious green fluorescence observed in the nanofiber precipitate. In contrast, the red fluorescence of Cy5-rituximab in the supernatant significantly decreased (with residual fluorescence possibly attributed to free Cy5 molecules) and appeared intensively in the nanofiber precipitate. Combined with the fluorescence spectra of the supernatants, the specificity of mimotope peptide nanofibers was mutually confirmed by a similar fluorescence change (Figure 4B). Subsequently, the HSA−rituximab protein mixture was used to further evaluate the specificity and anti-interference ability of the mimotope peptide nanofibers. As depicted in Figure 4C, HSA was detected in both the flow-through and washing fractions, indicating complete removal during loading and washing stages despite its concentration being four times that of rituximab. Consequently, only rituximab was observed in the elution fractions, confirming its capture by mimotope peptide nanofibers. Similarly, the capture of another anti-CD20 mAb (BAT 4306F) was successfully achieved by the mimotope peptide nanofibers (Figure S6). In contrast, the NBD-FFVLR nanofibers without recognition elements failed to capture rituximab. These findings illustrated the excellent specificity of the mimotope peptide nanofibers in capturing the target antibody without nonspecific adsorption onto HSA, highlighting their vast potential for applications in complex systems.

Applications of the Mimotope Peptide Nanofibers in Complex Biofluids. Clinical monitoring and in vivo metabolic research of mAbs rely on their capture from complex biofluids. Thus, the practical application of the mimotope peptide nanofibers was measured by enriching rituximab from two different spiked biosamples: cancer cell culture medium and human serum (Figure 5A). As depicted in Figure 5B, only rituximab was monitored in the elution fraction, and other interference proteins were present in the flowthrough and washing fractions. Then, it was further verified by QTOF MS (Figure S8) that the spectrum of the enriched rituximab was consistent with the characteristic spectrum of standard rituximab and did not contain interfering proteins. So, the mimotope peptide nanofibers can precisely enrich target rituximab from complex biofluids. Moreover, reproducibility was also verified according to the enrichment performances of five batches of mimotope peptide nanofibers (the recovery = 89%, RSD = 1.4%, Figure 5C,D). Considering that harsh chemical conditions and/or repetitive physical manipulations during enrichment may modify and inactivate the antibody, the second structure of the enriched rituximab was monitored by CD analysis (Figure 5E). The broad peak at 216 nm was attributed to the distinctive β-lamellar structure of rituximab, and no significant difference was observed between the CD spectra of the standard protein and the enriched rituximab. Therefore, the secondary structure of rituximab was maintained after enrichment. Based on these results, the mimotope peptide nanofibers showed great potential for efficient and rapid capture of antibodies from complex biofluids.

https://doi.org/10.1021/acs.analchem.4c00051
Anal. Chem. XXXX, XXX, XXX−XXX

More importantly, in vivo analysis of the mAb will face the challenge of more complex biofluids such as serum. Hence, the mimotope peptide nanofiber was tested to enrich rituximab from spiked 10% human serum. Owing to the superior specificity and selectivity, high affinity, and good enrichment performances of the mimotope peptide nanofibers, rituximab can be efficiently fished out, and most of the serum interference proteins were removed (Figure S9). Moreover, the peptide sequence coverage of the enriched rituximab was determined by LC-QTOF-MS after trypsin digestion. Similar results were obtained for the eluted rituximab (heavy chain 91.2%, light chain 95.8%) and standard rituximab (heavy chain 97.7%, light chain 99.6%, Figure 6A). We also investigated the potential of our approach for monitoring the posttranslational modifications (PTMs) of mAbs. Recently, some reports indicated that the modification of asparagine 55 at the heavy chain (HC-N55) of rituximab is a critical quality attribute for their quality control and biotransformation monitoring.[37,38] Therefore, after 21 day incubation, the deamidation of HC-N55 on rituximab was tracked by the enrichment of the mimotope peptide nanofibers, trypsin digestion, and LC-QTOF-MS analysis. As shown in Figure 6B,C, the deamidation of HC-N55 on rituximab increased from 9.9% (0 day) to 16.2% (incubated in serum for 21 days). These results further proved that the mimotope peptide nanofibers possess great application prospects for high-efficiency antibody enrichment in a complex biomatrix. Most of all, it is the first successful application of taking advantage of the peptide supramolecules to study antibody biotransformation. This may inspire the development of the field.

CONCLUSIONS

In this study, mimotope peptide derivative-based nanofibers were first developed according to the "polyvalent recognition" strategy, which could efficiently overcome the target binding barriers of traditional supramolecules. Moreover, these nanofibers can be rapidly formed within only 1 min. Their binding affinity for rituximab was found 38 times higher than that of the monomeric peptide. Additionally, these nanofibers exhibited an impressive "instantaneous capture" rate (within 15 s), a high recovery (93% ± 4%), and good specificity for target rituximab. Thanks to these properties, a substrate-free enrichment method, simple and quick (1 min for self-assembly; 15 s for mixing) was established, and the whole enrichment process could be completed in 30 min. The enrichment of rituximab was applied to cell culture medium with good yield and high batch to batch reproducibility. More importantly, the huge potential of the mimotope peptide nanofibers in biopharmaceutical analysis was confirmed by the tracking analysis of asparagine 55 deamidation (from 10% for 0 day to 16% for 21 day) on the heavy chain of rituximab in spiked human serum. In the future, by fine-tuning the functional units and hydrophilic−hydrophobic properties of mimotope peptide derivatives, it is expected to further improve the specificity for the target, as well as their bioactivity and functionality in the resultant nanofibers, for biomedical development. Additionally, this peptide self-assembly strategy shows potential for adaption to other target molecules by modifying the functional module. The primary challenge in designing for a new target molecule lies in regulating peptide sequences to control self-assembly. Biomimetic assembly design, superstructure screening, and prediction based on the computer simulation technology may be the key to accelerate the development of such peptide supramolecules.

ASSOCIATED CONTENT

Supporting Information

The Supporting Information is available free of charge at https://pubs.acs.org/doi/10.1021/acs.analchem.4c00051.

Materials and instruments; methods for CAC measurement, CG simulations, enrichment of rituximab using the nanofibers from the HSA−rituximab mixture and the SEC analysis; table for CAC comparison of currently reported self-assembling peptides; table for performance comparison of reported affinity materials about antibody enrichment in recent years; cosolvent optimization of the mimotope peptide derivatives; excitation and emission spectra of the mimotope peptide derivatives; CG simulation for the rapid self-assembly process of the mimotope peptide derivatives; internal interactions analysis of mimotope peptide nanofibers based on CG simulations; morphology identification of the mimotope peptide nanofibers after overnight self-assembly under TEM; further specificity assay of the mimotope peptide nanofibers; original fluorescence images of different components obtained by precipitation of FITC−HSA and Cy5-rituximab with mimotope peptide nanofibers; the determination of intact molecular mass for standard rituximab and the elution of spiked cell culture medium by ZenoTOF 7600 Mass; SDS-PAGE analysis of enrichment for rituximab using the mimotope peptide nanofibers from 10% human serum (PDF)

AUTHOR INFORMATION

Corresponding Authors

Yingchun Li − *School of Science, Harbin Institute of Technology, Shenzhen, Guangdong 518055, China;* orcid.org/0000-0002-5371-3587; Email: liyingchun@hit.edu.cn

Qiqin Wang − *Institute of Pharmaceutical Analysis, College of Pharmacy/State Key Laboratory of Bioactive Molecules and Druggability Assessment/International Cooperative Laboratory of Traditional Chinese Medicine Modernization and Innovative Drug Development of Ministry of Education (MOE) of China, Jinan University, Guangzhou 510632, China*; Email: qiqinxtu@163.com

Zhengjin Jiang − *Institute of Pharmaceutical Analysis, College of Pharmacy/State Key Laboratory of Bioactive Molecules and Druggability Assessment/International Cooperative Laboratory of Traditional Chinese Medicine Modernization and Innovative Drug Development of Ministry of Education (MOE) of China, Jinan University, Guangzhou 510632, China;* orcid.org/0000-0002-5612-4331; Email: jzjjackson@hotmail.com

Authors

Qiaoxian He − *Institute of Pharmaceutical Analysis, College of Pharmacy/State Key Laboratory of Bioactive Molecules and Druggability Assessment/International Cooperative Laboratory of Traditional Chinese Medicine Modernization and Innovative Drug Development of Ministry of Education (MOE) of China, Jinan University, Guangzhou 510632, China*

https://doi.org/10.1021/acs.analchem.4c00051
Anal. Chem. XXXX, XXX, XXX−XXX

Feng Chen − *Institute of Pharmaceutical Analysis, College of Pharmacy/State Key Laboratory of Bioactive Molecules and Druggability Assessment/International Cooperative Laboratory of Traditional Chinese Medicine Modernization and Innovative Drug Development of Ministry of Education (MOE) of China, Jinan University, Guangzhou 510632, China*

Zheng Zhao − *Institute of Pharmaceutical Analysis, College of Pharmacy/State Key Laboratory of Bioactive Molecules and Druggability Assessment/International Cooperative Laboratory of Traditional Chinese Medicine Modernization and Innovative Drug Development of Ministry of Education (MOE) of China, Jinan University, Guangzhou 510632, China*

Pengfei Pei − *Beijing Key Laboratory of Bioprocess, College of Life Science and Technology, Beijing University of Chemical Technology, Beijing 100029, P. R. China*

Yongqing Gan − *School of Basic Medicine and Clinical Pharmacy, China Pharmaceutical University, Nanjing 210009, China*

Aixuan Zhou − *Institute of Pharmaceutical Analysis, College of Pharmacy/State Key Laboratory of Bioactive Molecules and Druggability Assessment/International Cooperative Laboratory of Traditional Chinese Medicine Modernization and Innovative Drug Development of Ministry of Education (MOE) of China, Jinan University, Guangzhou 510632, China*

Jingwei Zhou − *Institute of Pharmaceutical Analysis, College of Pharmacy/State Key Laboratory of Bioactive Molecules and Druggability Assessment/International Cooperative Laboratory of Traditional Chinese Medicine Modernization and Innovative Drug Development of Ministry of Education (MOE) of China, Jinan University, Guangzhou 510632, China*

Jia-Huan Qu − *Institute of Pharmaceutical Analysis, College of Pharmacy/State Key Laboratory of Bioactive Molecules and Druggability Assessment/International Cooperative Laboratory of Traditional Chinese Medicine Modernization and Innovative Drug Development of Ministry of Education (MOE) of China, Jinan University, Guangzhou 510632, China*

Jacques Crommen − *Institute of Pharmaceutical Analysis, College of Pharmacy/State Key Laboratory of Bioactive Molecules and Druggability Assessment/International Cooperative Laboratory of Traditional Chinese Medicine Modernization and Innovative Drug Development of Ministry of Education (MOE) of China, Jinan University, Guangzhou 510632, China; Laboratory for the Analysis of Medicines, Department of Pharmaceutical Sciences, CIRM, University of Liege, B-4000 Liege, Belgium*

Marianne Fillet − *Institute of Pharmaceutical Analysis, College of Pharmacy/State Key Laboratory of Bioactive Molecules and Druggability Assessment/International Cooperative Laboratory of Traditional Chinese Medicine Modernization and Innovative Drug Development of Ministry of Education (MOE) of China, Jinan University, Guangzhou 510632, China; Laboratory for the Analysis of Medicines, Department of Pharmaceutical Sciences, CIRM, University of Liege, B-4000 Liege, Belgium;* orcid.org/0000-0002-1453-6282

Complete contact information is available at: https://pubs.acs.org/10.1021/acs.analchem.4c00051

Author Contributions

Qiaoxian He: investigation, experimentation, methodology, and writing—original draft. **Feng Chen**: experimentation. **Zheng Zhao**: experimentation. **Pengfei Pei**: experimentation. **Yongqing Gan**: ancillary analysis of peptide self-assembly. **Aixuan Zhou**: experimentation. **Jingwei Zhou**: experimentation. **Jia-Huan Qu**: writing—review and editing. **Jacques Crommen**: writing—review and editing. **Marianne Fillet**: writing—review and editing. **Yingchun Li**: writing—review and editing, research guidance, supervision, and resources. **Zhengjin Jiang**: writing—review and editing, supervision, resources, and funding acquisition. **Qiqin Wang**: conceptualization, writing—original draft, writing—review and editing, supervision, resources, and funding acquisition.

Notes

The authors declare no competing financial interest.

■ ACKNOWLEDGMENTS

This work was supported by the National Natural Science Foundation of China (82373829, 82273893, and 82173773), the Natural Science Foundation of Guangdong Province, China (2021A1515220099 and 2022A1515011576), the High-End Foreign Experts Project, China (G202119005L), and the Science and Technology Program of Guangdong Provincial Medical Products Administration, China (2023TDZ11, 2022ZDB04).

■ REFERENCES

(1) Levin, A.; Hakala, T. A.; Schnaider, L.; Bernardes, G. J. L.; Gazit, E.; Knowles, T. P. J. *Nat. Rev. Chem* **2020**, *4*, 615−634.
(2) Wang, M. D.; Lv, G. T.; An, H. W.; Zhang, N. Y.; Wang, H. *Angew. Chem., Int. Ed.* **2022**, *61*, No. e2021136.
(3) Wang, M. D.; Hou, D. Y.; Lv, G. T.; Li, R. X.; Hu, X. J.; Wang, Z. J.; Zhang, N. Y.; Yi, L.; Xu, W. H.; Wang, H. *Biomaterials* **2021**, *278*, 121139.
(4) Wu, Y.; Wen, H.; Bernstein, Z. J.; Hainline, K. M.; Blakney, T. S.; Congdon, K. L.; Snyder, D. J.; Sampson, J. H.; Sanchez-Perez, L.; Collier, J. H. *Sci. Adv.* **2022**, *8*, No. eabm7833.
(5) Li, Y.; Lock, L. L.; Wang, Y.; Ou, S. H.; Stern, D.; Schön, A.; Freire, E.; Xu, X.; Ghose, S.; Li, Z. J.; Cui, H. *Biomaterials* **2018**, *178*, 448−457.
(6) Li, Y.; Lock, L. L.; Mills, J.; Ou, B. S.; Morrow, M.; Stern, D.; Wang, H.; Anderson, C. F.; Xu, X.; Ghose, S.; Li, Z. J.; Cui, H. *Nano Lett.* **2020**, *20*, 6957−6965.
(7) Feng, Z.; Zhang, T.; Wang, H.; Xu, B. *Chem. Soc. Rev.* **2017**, *46*, 6470−6479.
(8) Li, Q.; Min, J.; Zhang, J.; Reches, M.; Shen, Y.; Su, R.; Wang, Y.; Qi, W. *Angew. Chem., Int. Ed.* **2023**, *62*, No. e202309830.
(9) Li, L. L.; Qiao, Z. Y.; Wang, L.; Wang, H. *Adv. Mater.* **2019**, *31*, 1804971.
(10) Li, T.; Lu, X. M.; Zhang, M. R.; Hu, K.; Li, Z. *Bioact. Mater.* **2022**, *11*, 268−282.
(11) Wang, J.; Liu, K.; Xing, R.; Yan, X. *Chem. Soc. Rev.* **2016**, *45*, 5589−5604.
(12) Wang, J.; Li, Y.; Nie, G. *Nat. Rev. Mater.* **2021**, *6*, 766−783.
(13) An, H. W.; Li, L. L.; Wang, Y.; Wang, Z.; Hou, D.; Lin, Y. X.; Qiao, S. L.; Wang, M. D.; Yang, C.; Cong, Y.; Ma, Y.; Zhao, X. X.; Cai, Q.; Chen, W. T.; Lu, C. Q.; Xu, W.; Wang, H.; Zhao, Y. *Nat. Commun.* **2019**, *10*, 4861.
(14) An, H. W.; Mamuti, M.; Wang, X.; Yao, H.; Wang, M. D.; Zhao, L.; Li, L. L. *Exploration* **2021**, *1*, 20210153.
(15) Han, S.; Cao, S.; Wang, Y.; Wang, J.; Xia, D.; Xu, H.; Zhao, X.; Lu, J. R. *Chem.—Eur. J.* **2011**, *17*, 13095−13102.
(16) Zhang, L.; Jing, D.; Jiang, N.; Rojalin, T.; Baehr, C. M.; Zhang, D.; Xiao, W.; Wu, Y.; Cong, Z.; Li, J. J.; Li, Y.; Wang, L.; Lam, K. S. *Nat. Nanotechnol.* **2020**, *15*, 145−153.

(17) Knowles, T. P.; Fitzpatrick, A. W.; Meehan, S.; Mott, H. R.; Vendruscolo, M.; Dobson, C. M.; Welland, M. E. *Science* **2007**, *318*, 1900−1903.
(18) Huang, S.; Wang, W.; Li, J.; Zhang, T.; Liang, Y.; Wang, Q.; Jiang, Z. *Chem. Eng. J.* **2021**, *419*, 129613.
(19) Huang, S.; Tang, R.; Zhang, T.; Zhao, J.; Jiang, Z.; Wang, Q. *Biosens. Bioelectron.* **2021**, *171*, 112678.
(20) Lu, L.; Liu, X.; Zuo, C.; Zhou, J.; Zhu, C.; Zhang, Z.; Fillet, M.; Crommen, J.; Jiang, Z.; Wang, Q. *Anal. Chim. Acta* **2022**, *1225*, 340199.
(21) Lei, Y.; Liu, X.; Lu, L.; Liu, C.; Xu, R.; Huang, S.; Shen, Y.; Deng, C.; Yu, J.; Zhang, T.; Crommen, J.; Wang, Q.; Jiang, Z. *J. Chromatogr. A* **2020**, *1632*, 461607.
(22) Lei, Y.; Shen, Y.; Zuo, C.; Lu, L.; Crommen, J.; Wang, Q.; Jiang, Z. *TrAC, Trends Anal. Chem.* **2022**, *157*, 116744.
(23) Mammen, M.; Choi, S. K.; Whitesides, G. M. *Angew. Chem., Int. Ed.* **1998**, *37*, 2754−2794.
(24) Men, D.; Zhou, J.; Li, W.; Wei, C. H.; Chen, Y. Y.; Zhou, K.; Zheng, Y.; Xu, K.; Zhang, Z. P.; Zhang, X. E. *ACS Appl. Mater. Interfaces* **2018**, *10*, 41019−41025.
(25) Fan, J. Q.; Li, Y. J.; Wei, Z. J.; Fan, Y.; Li, X. D.; Chen, Z. M.; Hou, D. Y.; Xiao, W. Y.; Ding, M. R.; Wang, H.; Wang, L. *Nano Lett.* **2021**, *21*, 6202−6210.
(26) Hu, X. X.; He, P. P.; Qi, G. B.; Gao, Y. J.; Lin, Y. X.; Yang, C.; Yang, P. P.; Hao, H.; Wang, L.; Wang, H. *ACS Nano* **2017**, *11*, 4086−4096.
(27) Yang, P. P.; Li, Y. J.; Cao, Y.; Zhang, L.; Wang, J. Q.; Lai, Z.; Zhang, K.; Shorty, D.; Xiao, W.; Cao, H.; Wang, L.; Wang, H.; Liu, R.; Lam, K. S. *Nat. Commun.* **2021**, *12*, 4494.
(28) König, N.; Szostak, S. M.; Nielsen, J. E.; Dunbar, M.; Yang, S.; Chen, W.; Benjamin, A.; Radulescu, A.; Mahmoudi, N.; Willner, L.; Keten, S.; Dong, H.; Lund, R. *ACS Nano* **2023**, *17*, 12394−12408.
(29) Cui, T.; Li, X.; He, S.; Xu, D.; Yin, L.; Huang, X.; Deng, S.; Yue, W.; Zhong, W. *ACS Biomater. Sci. Eng.* **2020**, *6*, 5001−5011.
(30) Chen, Z.; Zhu, C.; Yang, J.; Zhang, M.; Yuan, J.; Shen, Y.; Zhou, J.; Huang, H.; Xu, D.; Crommen, J.; Jiang, Z.; Wang, Q. *Anal. Chem.* **2023**, *95*, 3532−3543.
(31) Yang, J.; Zhou, A.; Li, M.; He, Q.; Zhou, J.; Crommen, J.; Wang, W.; Jiang, Z.; Wang, Q. *Acta Pharm. Sin. B* **2024**, *14*, 1317−1328.
(32) Arabi, M.; Ostovan, A.; Zhang, Z.; Wang, Y.; Mei, R.; Fu, L.; Wang, X.; Ma, J.; Chen, L. *Biosens. Bioelectron.* **2021**, *174*, 112825.
(33) Arora, S.; Saxena, V.; Ayyar, B. V. *Methods* **2017**, *116*, 84−94.
(34) Padwal, P.; Finger, C.; Fraga-García, P.; Kaveh-Baghbaderani, Y.; Schwaminger, S. P.; Berensmeier, S. *ACS Appl. Mater. Interfaces* **2020**, *12*, 39967−39978.
(35) Kaveh-Baghbaderani, Y.; Allgayer, R.; Schwaminger, S. P.; Fraga-García, P.; Berensmeier, S. *ACS Appl. Nano Mater.* **2021**, *4*, 4956−4963.
(36) Tehrani Najafian, F.; Bibi, N. S.; Islam, T.; Fernández-Lahore, M. *Electrophoresis* **2017**, *38*, 2914−2921.
(37) Nupur, N.; Rathore, A. S. *J. Sep. Sci.* **2022**, *45*, 2887−2900.
(38) Di Marco, F.; Berger, T.; Esser-Skala, W.; Rapp, E.; Regl, C.; Huber, C. G. *Int. J. Mol. Sci.* **2021**, *22*, 9072.

https://doi.org/10.1021/acs.analchem.4c00051
Anal. Chem. XXXX, XXX, XXX−XXX